Unsteady Lift and Drag Forces Acting on the Elliptic Cylinder

Moon-Sang Kim*
School of Aerospace and Mechanical Engineering, Hankuk Aviation University, Kyungki-Do 412-791, Korea
Young-Bin Park
Graduate Student, Department of Aerospace Engineering, Hankuk Aviation University, Kyungki-Do 412-791, Korea

A parametric study has been accomplished to figure out the effects of elliptic cylinder thickness, angle of attack, and Reynolds number on the unsteady lift and drag forces exerted on the elliptic cylinder. A two-dimensional incompressible Navier-Stokes flow solver is developed based on the SIMPLER method in the body-intrinsic coordinates system to analyze the unsteady viscous flow over elliptic cylinder. Thickness-to-chord ratios of 0.2, 0.4, and 0.6 elliptic cylinders are simulated at different Reynolds numbers of 400 and 600, and angles of attack of 10°, 20°, and 30°. Through this study, it is observed that the elliptic cylinder thickness, angle of attack, and Reynolds number are very important parameters to decide the lift and drag forces. All these parameters also affect significantly the frequencies of the unsteady force oscillations.

Key Words : Unsteady Force, SIMPLER Method, Elliptic Cylinder, Navier-Stokes Equations Incompressible Viscous Flow, Angle of Attack

1. Introduction

The flow field around a blunt body has some significant flow phenomena. The vortex shedding behind a blunt body is one of them. The alternate vortex shedding occurred in the near wake behind a blunt body leads to periodically oscillating lift and drag forces. The periodicity of the wake of a blunt body is associated with the formation of a stable street of staggered vortices by von Kármán (1912). In his paper, he analyzed the stability of vortex street configurations and established a theoretical link between the vortex street structure and the drag on the body.

* Corresponding Author,
E-mail : mskim@hau.ac.kr
TEL : +82-2-300-0285; **FAX** : +82-2-3158-4429
School of Aerospace and Mechanical Engineering, Hankuk Aviation University, Kyungki-Do 412-791, Korea. (Manuscript **Received** September 2, 2005; **Revised** December 1, 2005)

The oscillating lift force, whose direction is transverse to the flow, is especially large and may cause structural vibrations, acoustic noise, or resonance, which in some cases can trigger failure (Williamson, 1996). The Tacoma Narrows suspension bridge disaster is a good example, which was collapsed due to wind induced vibrations on November 7, 1940.

Since then, many researchers have studied unsteady flows past blunt bodies, especially circular cylinders. Jordan and Fromm (1972) investigated oscillatory drag, lift, and torque on a circular cylinder in a uniform flow at Reynolds numbers of 100, 400, and 1,000 by solving vorticity-stream function formulation. They showed the dramatic rise of the drag coefficient during the development of the Kármán vortex street. A detailed study of the wake structures and flow dynamics associated with simulated two-dimensional flows past a circular cylinder that is either stationary or in simple harmonic cross-flow oscillation is done by Blackburn and Henderson (1999). Also,

numerical algorithm development has been accomplished by many researchers. Manzari (2003) presented a finite element solution procedure for the simulation of transient incompressible fluid flows using triangular meshes. His algorithm is based on the artificial compressibility technique in connection with a dual time-stepping approach. A higher-order immersed boundary method was applied to the two-dimensional unsteady incompressible Navier-Stokes equations in vorticity-stream function formulation to solve the unsteady incompressible flow by Linnick and Fasel (2003).

Actually, many studies have been accomplished for flows past circular cylinders because of geometric simplicity. However, it would be valuable attempts to study the flows past elliptic cylinders. Engineering applications often involve flows over complex bodies like wings, submarines, missiles, and rotor blades, which can hardly be modeled as a flow over a circular cylinder. In such flows, cylinder thickness and angle of attack can greatly influence the nature of separation and the wake structure (Mittal and Balachandar, 1996).

In 1987, Ota et al.(1987) investigated a flow around an elliptic cylinder of axis ratio 1 : 3 in the critical Reynolds number regime, which extends from about Re=85,000 to 312,000, on the basis of mean static pressure measurements along the cylinder surface and of hot-wire velocity measurements in the near wake. Nair and Sengupta (1996) solved Navier-Stokes equations in order to study the onset of computed asymmetry around elliptic cylinders at a Reynolds number of 10,000. They found that the ellipses developed asymmetry much earlier than the circular cylinder. Kim and Sengupta (2005) studied unsteady flow past an elliptic cylinder whose axis ratios are 0.6, 0.8, 1.0, and 1.2 at different Reynolds numbers of 200, 400, and 1,000 to investigate the unsteady lift and drag forces. They found that the elliptic cylinder thickness and Reynolds number can affect significantly the frequencies of the force oscillations as well as the mean values and the amplitudes of the drag and lift forces.

Investigations of incident angle effect also have been done by many people. Patel (1981) investigated the incompressible viscous flow around an impulsively started elliptic cylinder at 0°, 30°, 45° and 90° incidences and at the Reynolds numbers of 100 and 200. He solved the system of coupled partial differential equations which were obtained by substituting the expanded finite Fourier series of the stream and vorticity functions in the Navier-Stokes equations. Chou and Huang (1996) proposed a semi-explicit finite difference scheme to study the unsteady two-dimensional incompressible flow past a bluff object at high Reynolds numbers up to 40,000. They considered the aspect ratio and angle of attack as controlled parameters. In 2001, Badr et al. (2001) used a series truncation method based on Fourier series to reduce the Navier-Stokes equations. The Reynolds number range was up to 5,000 and axis ratios of the elliptic cylinder were between 0.5 and 0.6, and angle of attack ranges between 0° and 90°. They showed an unusual phenomenon of negative lift occurring shortly after the start of motion.

The objective of the present research is to study the effects of elliptic cylinder thickness, angle of attack, and Reynolds number on the unsteady lift and drag forces exerted on the body by solving unsteady form of incompressible Navier-Stokes equations in the body-intrinsic orthogonal curvilinear coordinate system using SIMPLER method in conjunction with Crank-Nicolson time integration scheme. Unsteady incompressible viscous flow past an elliptic cylinder is simulated at various thickness-to-chord ratios of 0.2, 0.4, and 0.6. The Reynolds numbers of 400, 600 and the angles of attack of 10°, 20°, and 30° are considered as parameters in this research.

2. Flow Solver Development

2.1 Governing equations

For the present analysis, the flow field is assumed to be unsteady, incompressible, laminar flow. The coordinate system is taken to be a two-dimensional, body-intrinsic, orthogonal curvilinear coordinate system as shown in Fig. 1 wherein the ξ-direction is taken to be along the body while the η-direction is perpendicular to

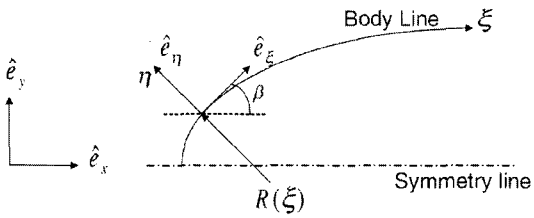

Fig. 1 Two-dimensional body-intrinsic coordinate system

the body surface. Here, $R(\xi)$ is the radius of curvature at point ξ. With these assumptions, continuity and momentum equations can be expressed as follows and detailed derivation can be found in Reference Lim (1991).

Continuity Equation :

$$\frac{\partial \rho}{\partial t}+\frac{1}{h_1}\frac{\partial}{\partial \xi}(\rho v_\xi)+\frac{1}{h_1}\frac{\partial}{\partial \eta}(h_1 \rho v_\eta)=0$$

Here, the first term can be dropped for incompressible flow but it is retained here for convenience.

v_ξ-Momentum Equation :

$$\frac{\partial}{\partial t}(\rho v_\xi)+\frac{1}{h_1}\frac{\partial}{\partial \xi}\left(\rho v_\xi v_\xi-\frac{1}{h_1}\mu\frac{\partial v_\xi}{\partial \xi}\right)+\frac{1}{h_1}\frac{\partial}{\partial \eta}\left(h_1\rho v_\eta v_\xi-h_1\mu\frac{\partial v_\xi}{\partial \eta}\right)$$
$$=-\frac{1}{h_1}(\rho v_\xi v_\eta)\frac{\partial h_1}{\partial \eta}-\frac{1}{h_1}\frac{\partial p}{\partial \xi}+\frac{\mu}{h_1}\left[\frac{\partial}{\partial \xi}\left(\frac{v_\eta}{h_1}\frac{\partial h_1}{\partial \eta}\right)+\left(\frac{1}{h_1}\frac{\partial v_\eta}{\partial \xi}-\frac{v_\xi}{h_1}\frac{\partial h_1}{\partial \eta}\right)\frac{\partial h_1}{\partial \eta}\right]$$

v_η-Momentum Equation :

$$\frac{\partial}{\partial t}(\rho v_\eta)+\frac{1}{h_1}\frac{\partial}{\partial \xi}\left(\rho v_\xi v_\eta-\frac{1}{h_1}\mu\frac{\partial v_\eta}{\partial \xi}\right)+\frac{1}{h_1}\frac{\partial}{\partial \eta}\left(h_1\rho v_\eta v_\eta-h_1\mu\frac{\partial v_\eta}{\partial \eta}\right)$$
$$=\frac{1}{h_1}(\rho v_\xi v_\xi)\frac{\partial h_1}{\partial \eta}-\frac{\partial p}{\partial \eta}+\frac{\mu}{h_1}\left[\frac{\partial}{\partial \xi}\left(\frac{v_\xi}{h_1}\frac{\partial h_1}{\partial \eta}\right)-\left(\frac{1}{h_1}\frac{\partial v_\xi}{\partial \xi}-\frac{v_\eta}{h_1}\frac{\partial h_1}{\partial \eta}\right)\frac{\partial h_1}{\partial \eta}\right]$$

2.2 Computational domain and boundary conditions

The flow geometry along with the boundary conditions for the present work is shown in Fig. 2. The outer boundary of the computational domain has 30 times of the unit chord length distance from the center of an elliptic cylinder. Here, the chord length is defined as a straight line connecting the leading edge and trailing edge of the elliptic cylinder. The no-slip boundary conditions are imposed on the solid surface and the free stream conditions are applied to the inflow

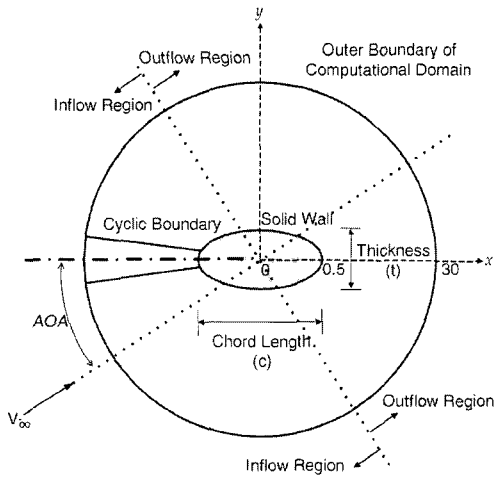

Fig. 2 Flow geometry and computational domain

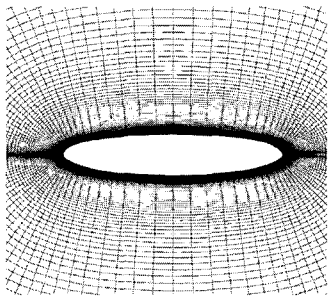

(a) $t/c=0.2$

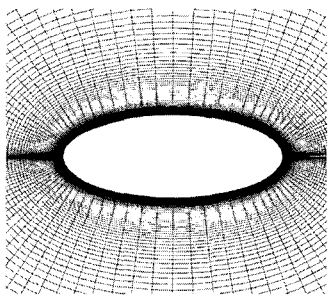

(b) $t/c=0.4$

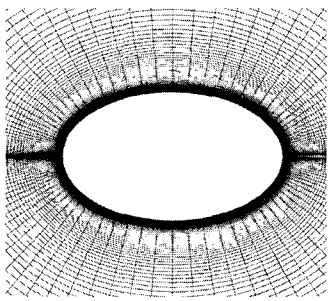

(c) $t/c=0.6$

Fig. 3 Elliptic cylinder grid near the body surface

boundary condition. The outflow boundary conditions are extrapolated from the interior grid point values. A cyclic boundary condition is also implemented to see the unsteady flow physics such as vortex shedding past an elliptic cylinder.

The O-mesh shaped 148×151 grid is generated algebraically and displayed in Fig. 3 for the three different thickness cases. Here, the chord length is taken as unit length and the maximum thickness is varied from 0.2 to 0.6.

2.3 Flow solver verification

Flow solver verification was accomplished and tabulated by one of the current authors in his previous work (Kim and Sengupta, 2005), so that part is omitted here.

3. Numerical Results and Discussions

The main purpose of this research is to figure out the effects of parameters, which are related with flow conditions such as angle of attack or Reynolds number and with geometry condition such as elliptic cylinder thickness, on the unsteady forces. Therefore, we focused our attention on the analysis of the numerical results instead of digging out the flow phenomena.

Figure 4(a) shows the typical lift (Cl) and drag (Cd) coefficient variations as a function of time (T) for the elliptic cylinder at Reynolds number of 600. The maximum thickness of the elliptic cylinder is taken as 60% of the unit chord length and the angle of attack is 10°. Here, the lift and drag coefficients are defined respectively as $Cl=2L/(\rho U_\infty^2 c)$ and $Cd=2D/(\rho U_\infty^2 c)$, where L, D, U_∞, and c are the lift force per unit span, drag force per unit span, free stream velocity, and the chord length of the elliptic cylinder, respectively. Also, the dimensionless time T is defined as $T=t/(c/U_\infty)$, where t is dimensional time. In this figure, oscillating frequencies and amplitudes of both coefficients can be compared very clearly. The amplitude of Cl is much greater than that of Cd, and the frequency of Cl is one-half the frequency of Cd. The frequency of Cl due to the vortex shedding can be expressed by Strouhal number (St), which is made dimensionless with the free stream velocity and the chord length of the elliptic cylinder such that $St=(fc/U_\infty)$, where f is frequency of lift force oscillation.

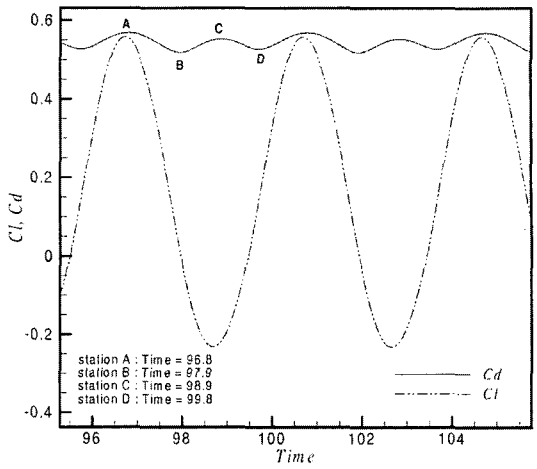

(a) Time history of lift and drag coefficient

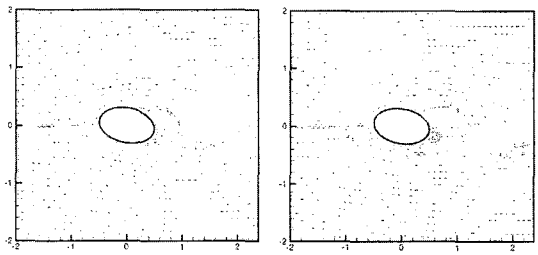

(b) Station A (c) Station B

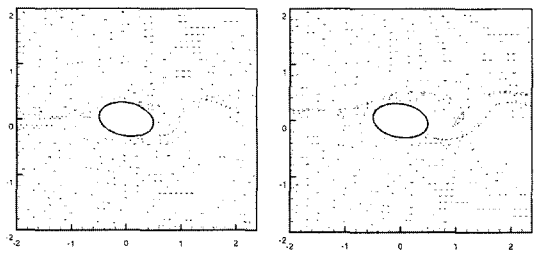

(d) Station C (e) Station D

Fig. 4 Typical Cl, Cd time history and streamline pattern ($t/c=0.6$, $Re=600$, AOA=10 deg)

Figure 4(b) to (e) shows a close-up look at a bottom shed to top shed cycle. When the vortex shedding occurs at the bottom of the cylinder (say, station A), the maximum Cd takes place and Cl has the almost maximum positive value at this station. After one period of drag force oscillation (say, station C), the maximum Cd

takes place again with the almost maximum negative value of Cl. The top vortex shedding occurs at this station.

The drag and lift forces exerted on the body may be decomposed into pressure force and friction force components as follows:

$$Cd=Cdp+Cdf,\ Cl=Clp+Clf$$

Here, Cdp and Cdf are the pressure and friction components of the drag coefficient, and Clp and Clf are the pressure and friction components of the lift coefficient, respectively.

Figures 5~7 plot the total time-averaged mean drag coefficient ($\overline{Cd}$), mean drag coefficient due to pressure ($\overline{Cdp}$), and mean drag coefficient due to friction ($\overline{Cdf}$) as a function of Reynolds number (Re) and angle of attack (AOA) at different thickness-to-chord ratio (t/c).

According to these figures, $\overline{Cd}$ and $\overline{Cdp}$ are increased as the angle of attack is increased. Also, they are increased as the cylinder thickness is thickened at the same angle of attack and Reynolds number. However, $\overline{Cd}$ is decreased as the Reynolds number increases whereas $\overline{Cdp}$ does not depend on the Reynolds number.

Figure 8 compares $\overline{Cdf}$ at different angles of attack, cylinder thickness, and Reynolds numbers. It is decreased as the angle of attack or Reynolds number is increased. However, it is increased as the

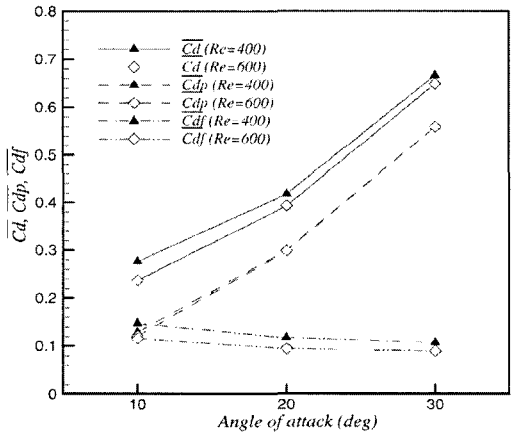

Fig. 5 $\overline{Cd}$, $\overline{Cdp}$, and $\overline{Cdf}$ at different angles of attack and Reynolds numbers (t/c=0.2)

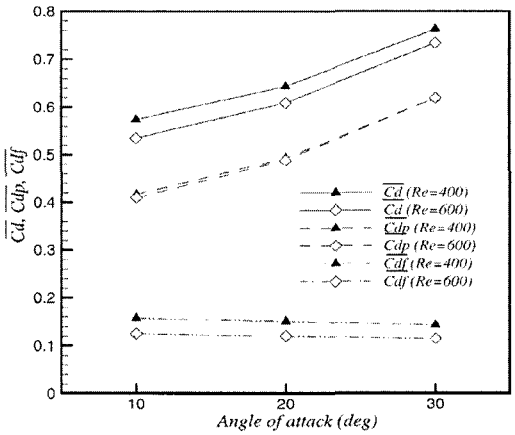

Fig. 7 $\overline{Cd}$, $\overline{Cdp}$, and $\overline{Cdf}$ at different angles of attack and Reynolds numbers (t/c=0.6)

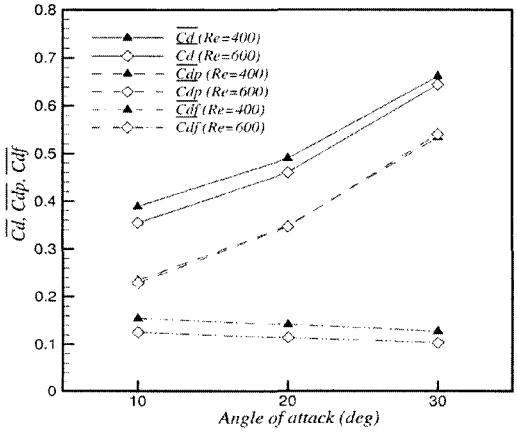

Fig. 6 $\overline{Cd}$, $\overline{Cdp}$, and $\overline{Cdf}$ at different angles of attack and Reynolds numbers (t/c=0.4)

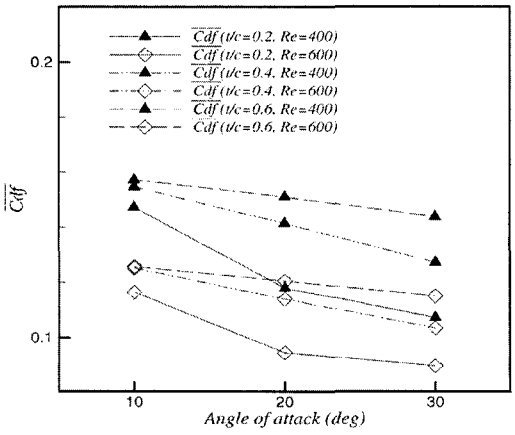

Fig. 8 $\overline{Cdf}$ at different angles of attack, cylinder thickness, and Reynolds numbers

cylinder thickness is thickened because of surface area increment.

Figures 9~11 plot the total time-averaged mean lift coefficient ($\overline{Cl}$), mean lift coefficient due to pressure ($\overline{Clp}$), and mean lift coefficient due to friction ($\overline{Clf}$) as a function of Reynolds number and angle of attack at different thickness-to-chord ratio.

In contrast to $\overline{Cd}$ and $\overline{Cdp}$, $\overline{Cl}$ and $\overline{Clp}$ are decreased as the cylinder thickness is thickened at the same angle of attack and Reynolds number although they are increased as the angle of attack is increased. It seems that the Reynolds number does not affect a lot $\overline{Cl}$ and $\overline{Clp}$. On the other hand, $\overline{Clf}$ does not depend on any parameters considered in this research. Its magnitude is almost equal to zero, so we can say that $\overline{Cl}$ is attributed to $\overline{Clp}$.

The oscillating amplitude of drag and lift coefficient gives a very important information in the unsteady flow physics. Figures 12~14 and Figs. 15~17 plot the amplitude of drag coefficient (ΔCd) and amplitude of lift coefficient (ΔCl) at different angles of attack, Reynolds numbers, and elliptic cylinder thickness. Here, the amplitudes of Cl and Cd oscillations are defined respectively as,

$$\Delta Cl=\frac{(Cl)_{max}-(Cl)_{min}}{2} \qquad \Delta Cd=\frac{(Cd)_{max}-(Cd)_{min}}{2}$$

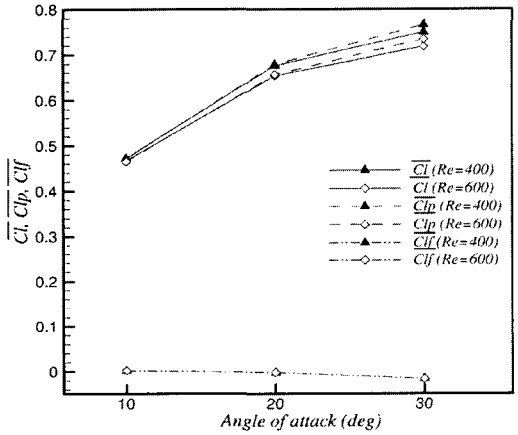

Fig. 9 $\overline{Cl}$, $\overline{Clp}$, and $\overline{Clf}$ at different angles of attack and Reynolds numbers (t/c=0.2)

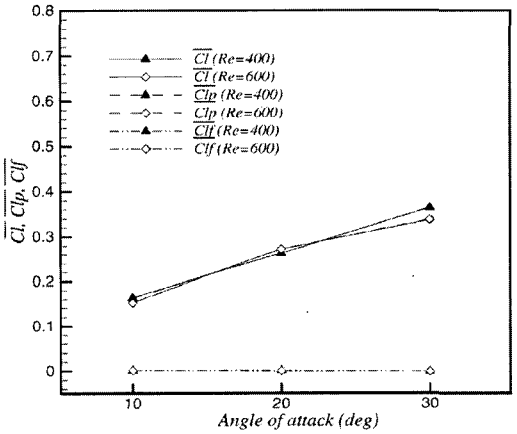

Fig. 11 $\overline{Cl}$, $\overline{Clp}$, and $\overline{Clf}$ at different angles of attack and Reynolds numbers (t/c=0.6)

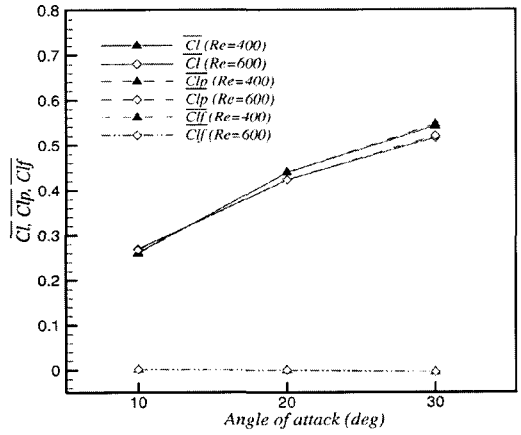

Fig. 10 $\overline{Cl}$, $\overline{Clp}$, and $\overline{Clf}$ at different angles of attack and Reynolds numbers (t/c=0.4)

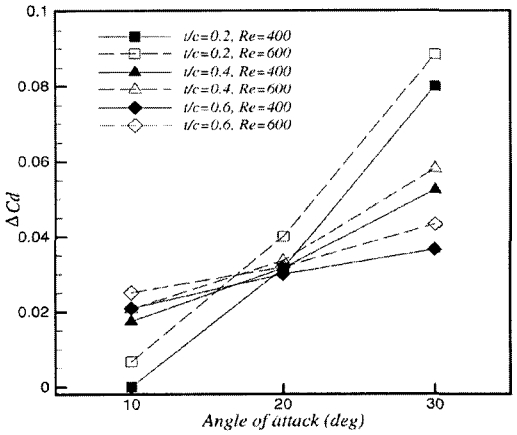

Fig. 12 Amplitude of Cd at different angles of attack

where the subscripts min and max denote the minimum and maximum values, respectively, in a period.

The amplitude of drag and lift coefficient is increased as the angle of attack is increased as shown in Figs. 12 and 15. Especially, the amplitude of drag force becomes more sensitive to the angle of attack when the cylinder thickness is thinner. Whereas the amplitude of drag force oscillation is decreased or increased depending on the angle of attack as the cylinder thickness is thickened as shown in Fig. 13, the amplitude of the lift force oscillation is increased as the cylinder thickness is thickened no matter what the angle of attack is as shown in Fig. 16. When the

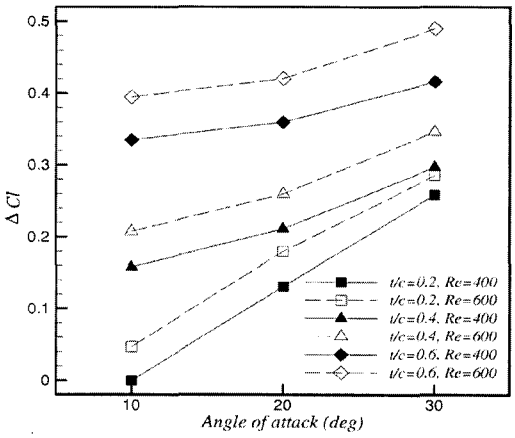

Fig. 15 Amplitude of Cl at different angles of attack

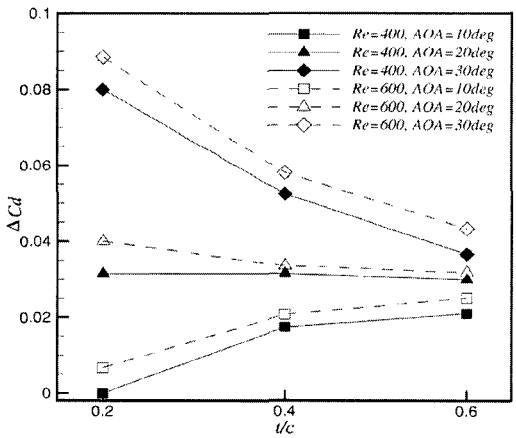

Fig. 13 Amplitude of Cd at different cylinder thickness

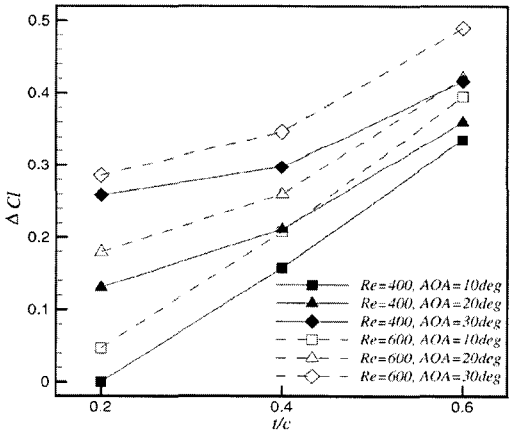

Fig. 16 Amplitude of Cl at different cylinder thickness

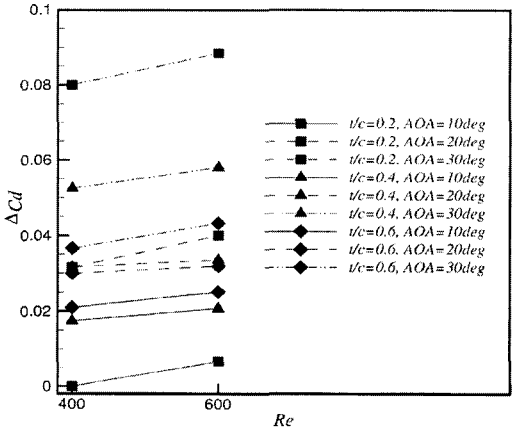

Fig. 14 Amplitude of Cd at different Reynolds numbers

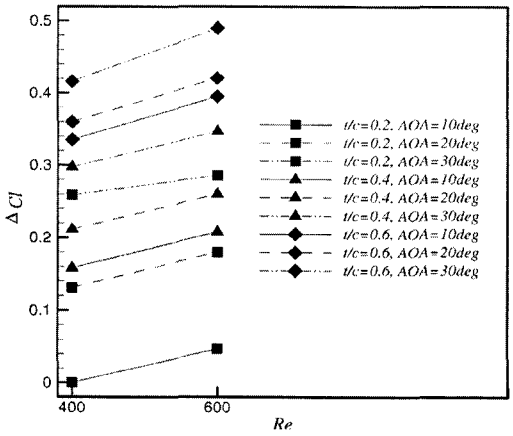

Fig. 17 Amplitude of Cl at different Reynolds numbers

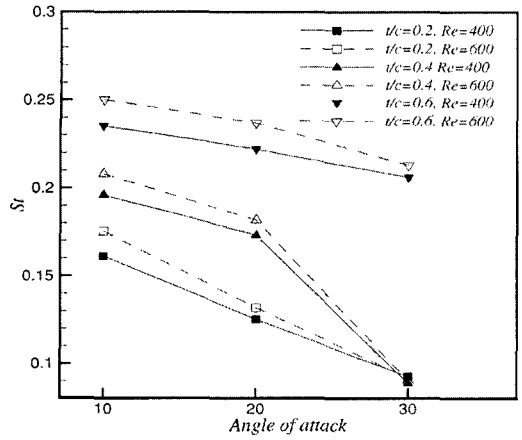

Fig. 18 Strouhal numbers at different angles of attack

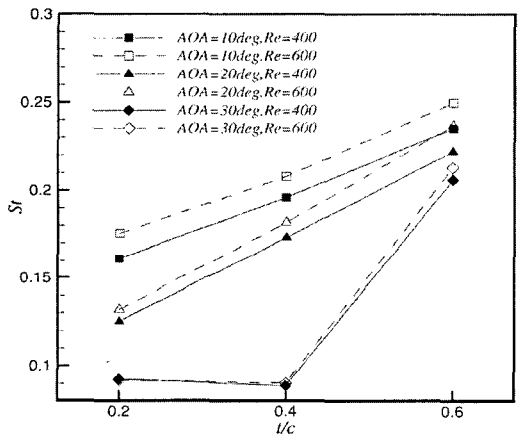

Fig. 19 Strouhal numbers at different cylinder thickness

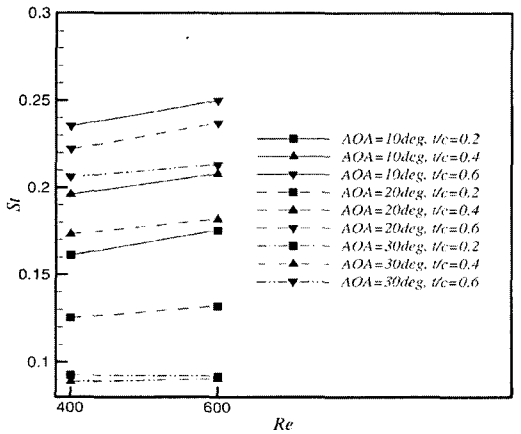

Fig. 20 Strouhal numbers at different Reynolds numbers

Reynolds number is increased, the amplitude of drag and lift force is also increased as shown in Figs. 14 and 17.

The Strouhal number, which represents the degree of lift force oscillation frequencies due to the periodic vortex shedding, is decreased as the angle of attack is increased as shown in Fig. 18. When the cylinder thickness is thickened, the Strouhal number is increased except for the case of $AOA=30°$ at $t/c=0.4$ as shown in Fig. 19. As the Reynolds number is increased, Strouhal number is increased a little bit more when the angle of attack is lower as shown in Fig. 20.

4. Summary and Conclusion

Through this parametric study, we conclude that all the parameters considered in this study have influence a lot on the unsteady forces induced by flow past an elliptic cylinder. The following conclusions can be used as a guideline to design the bodies such as airfoil, ship, submarines, train, trailer, etc.

(1) $\overline{Cd}$ can be reduced by decreasing the angle of attack or by making the cylinder thickness thinner. On the other hand, $\overline{Cl}$ can be increased by increasing the angle of attack or by making the cylinder thickness thinner. The increment of Reynolds number decreases $\overline{Cd}$ but does not much affect $\overline{Cl}$.

(2) The response of $\overline{Cdp}$ or $\overline{Clp}$ for the variations of the angles of attack or cylinder thickness has the same tendency as that of $\overline{Cd}$ or $\overline{Cl}$. However, both $\overline{Cdp}$ and $\overline{Clp}$ are not dependent on the Reynolds number variations.

(3) Although the response of $\overline{Cdf}$ for the variations of cylinder thickness or Reynolds numbers has the same tendency as that of $\overline{Cd}$, $\overline{Cdf}$ is decreased as the angle of attack is increased.

(4) $\overline{Clf}$ does not depend on the any parameters considered in this research and its magnitude is almost equal to zero.

(5) Both ΔCd and ΔCl are increased as the angle of attack is increased or Reynolds number is increased. Whereas ΔCd is increased or decreased depending on the angle of attack as the

cylinder thickness is thickened, ΔCl is increased as the cylinder thickness is thickened for the whole range of angles of attack.

(6) The Strouhal number is increased as the cylinder thickness is thickened (except high angle of attack) or Reynolds number is increased. But, it is decreased as the angle of attack is increased.

References

Badr, H. M., Dennis, S. C. R. and Kocabiyik, S., 2001, "Numerical Simulation of the Unsteady Flow Over an Elliptic Cylinder at Different Orientations," *International Journal for Numerical Methods in Fluids*, Vol. 37, pp. 905~931.

Blackburn, H. M. and Henderson, R. D., 1999, "A Study of Two-Dimensional Flow Past an Oscillating Cylinder," *Journal of Fluid Mechanics*, Vol. 385, pp. 255~286.

Chou, M. H. and Huang, W., 1996, "Numerical Study of High-Reynolds-Number Flow Past a Bluff Object," *International Journal for Numerical Methods in Fluids*, Vol. 23, pp. 711~732.

Jordan, S. K. and Fromm, J. E., 1972, "Oscillatory Drag, Lift and Torque on a Circular Cylinder in a Uniform Flow," *Physics of Fluids*, Vol. 15, No. 3, pp. 371~376.

Kármán, T., 1912, "Uber den Mechanismus des Widerstandes den ein bewegter Korper in einer Flussigkeit Erfahrt," *Nachr. Ges. Wiss. Gottingen, Math-Phys Klasse*, Vol. 12, pp. 509~517.

Kim, M. S. and Sengupta, A., 2005, "Unsteady Viscous Flow over Elliptic Cylinders At Various Thickness with Different Reynolds Numbers," *Journal of Mechanical Science and Technology*, Vol. 19, No. 3, pp. 877~886.

Lim, C. K., 1991, "Numerical Simulation of Non-lifting Flow Over Two-Dimensional Elliptic Cylinders," MS Thesis, Iowa State University.

Linnick, M. N. and Fasel, H. F., 2003, "A High-Order Immersed Boundary Method for Unsteady Incompressible Flow Calculations," *AIAA Paper* 2003~1124.

Manzari, M. T., 2003, "A Time-accurate Finite Element Algorithm for Incompressible Flow Problems," *International Journal of Numerical Methods for Heat & Fluid Flow*, Vol. 13, No. 2, pp. 158~177.

Mittal, R. and Balachandar, S., 1996, "Direct Numerical Simulation of Flow Past Elliptic Cylinders," *Journal of Computational Physics*, Vol. 124, pp. 351~367.

Nair, M. T. and Sengupta, T. K., 1996, "Onset of Asymmetry: Flow Past Circular and Elliptic Cylinders," *International Journal for Numerical Methods in Fluids*, Vol. 23, pp. 1327~1345.

Ota, T., Nishiyama, H. and Taoka, Y., 1987, "Flow Around an Elliptic Cylinder in the Critical Reynolds Number Regime," *Journal of Fluids Engineering*, Vol. 109, pp. 149~155.

Patel, V. A., 1981, "Flow Around the Impulsively Started Elliptic Cylinder at Various Angles of Attack," *Computers and Fluids*, Vol. 9, No. 4, pp. 435~462.

Williamson, C. H. K., 1996, "Vortex Dynamics in the Cylinder Wake," *Annual Review of Fluid Mechanics*, Vol. 28, pp. 477~539.